# POLITECNICO DI TORINO
## Repository ISTITUZIONALE

Acausal equation-based and object-oriented modeling of heating systems: The College Thermal library

(Article begins on next page)
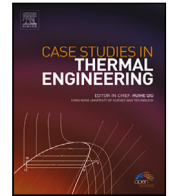
28 April 2024

# Acausal equation-based and object-oriented modeling of heating systems: The College Thermal library

Luigi Augello [a],[1], Ankit Naik [b],[1], Matteo Morciano [a], Jan Brugård [b],[*], Matteo Fasano [a],[*]

[a] *Department of Energy, Politecnico di Torino, Corso Duca degli Abruzzi 24, Torino, 10129, Italy*
[b] *Wolfram MathCore AB, Teknikringen 1E, Linköping, SE-583 30, Sweden*

## ARTICLE INFO

## ABSTRACT

With the growing demand for adequate thermal comfort and increasingly sophisticated and interconnected energy systems, software tools able to easily and effectively study complex thermal systems need to be developed. Here, a novel acausal equation-based and object-oriented modeling (OOM) approach is used to model the seasonal performance of a residential heating system taken as a case study. To this end, a purpose-built library named *College Thermal* was developed using *Modelica* language in the *Wolfram System Modeler* simulation environment. In detail, dynamic simulations under varying operating conditions were performed to assess the ability of the system to ensure the design conditions, and to estimate the resulting energy consumption during the heating season. Then, the effect of key parameters of the thermal components on the overall energy performance of the system is analyzed. The developed OOM library, which is characterized by interoperability, modularity, and scalability features and thus could easily incorporate extensions/evolutions of the studied system, would be prospectively suitable for optimizing system layouts and testing control strategies in various thermal engineering applications.

## 1. Introduction

Zero-energy building is becoming a worldwide trend due to the increasing demand for sustainable thermo-hygrometric comfort and thus reduction in carbon footprint [1–3]. In this context, a proper sizing of heating, ventilation and air conditioning (HVAC) systems for buildings is fundamental, both to ensure an adequate comfort for the occupants and to realize efficient systems complying with increasingly rigorous environmental standards [4].

The need to ensure specific energy performance led to the development and widespread of a large number of system modeling techniques, which are able to account for the technical specifications and operating conditions of HVAC systems. Such factors may belong to different domains such as thermodynamic, fluid-mechanic, electrical, and control ones [5]. Among these modeling techniques, the acausal equation-based and object-oriented modeling approach (OOM) is emerging as a promising one [6]. Contrary to the assignment statement- and block-based approaches, where the users have to (i) decide on input and output signals for the system, (ii) set-up the system of equations, (iii) derive the output as a function of the input and (iv) create the model, the OOM approach does not require the knowledge of a predetermined causal algorithm to perform calculations on complex systems. In fact, in such a modern simulation environment, the individual components of the model describe the equations directly and not the

algorithm of their solution. Thus, one of the key strengths lies in the potential to break down a complex model into simpler sub-components, each of these mathematically described by a set of equations. Specific ports, called *pins*, allow studying interconnected components from different domains, thus enabling key variables to interact and mimicking real-world topology. Due to these advantages, the OOM approach lends itself perfectly to the challenge of dynamically modeling complex thermal systems [7,8].

Many codes based on OOM approach were already developed for the simulation of engineering systems, such as: *APMonitor*, *ASCEND* and *Modelica* [9,10]. For instance, Hawila and co-workers [11] modeled a radiant floor heating system through *Modelica* language in the well-known *Dymola* simulation environment [12–14]. Instead, Franke [15] investigated a solar heating system located in Särö (southern Sweden), where the overall model was composed by three interacting sub-models: a load sub-system, a solar collector and a heat storage device. All the aforementioned components were modeled through *Omola* and simulated in *OMSim* environment.

In this work, an heating system for residential building was modeled using the OOM approach via *Wolfram System Modeler* for the first time. *Wolfram System Modeler* is an interactive graphical simulation environment based on *Modelica* language [6,8], where the user can create multi-domain system models using an extensive library of ready-to-use physical and logical components, following a drag and drop approach. The components are thus reusable, allowing to quickly explore alternative designs and scenarios, leading to a flexible and modular approach [16]. Moreover, *Wolfram System Modeler* and the *Wolfram Language* are fully integrated, enabling modelers to analyze, understand and quickly iterate system designs. In detail, the specific case study of heating system addressed here is made of a heat pump, fan coils terminals, and a network of pipes (water is considered as heat transfer fluid). We chose an air–water heat pump as heat supplier since heat pumps have been lately recognized as key clean energy technologies in the energy transition, especially when existing centralized systems based on fossil fuels are substituted [17,18]. The studied heating system was coupled with the dynamic thermal model of the building, which allowed investigating how variation of certain technical or environmental parameters may affect dynamically the required thermal power. In order to create the whole model, the *College Thermal* library, containing all the aforementioned sub-components, was created *ad hoc* and deployed in the *Wolfram System Modeler* repository [19].

## 2. Methodology

A case study heating system for residential building was dynamically modeled to test the capabilities of the *Wolfram System Modeler* environment. First, the heat power required by each room to guarantee the desired indoor thermal comfort was calculated, according to the considered boundary conditions. To this purpose, the various elements of a room, such as walls, windows, doors, floor and roof, were modeled developing built-in components in the *College Thermal* library (which is based on *Modelica* language). These components were then properly connected together to realistically define the physical model of a generic room. Several heat losses/sources were considered in this block, such as thermal transfer through both opaque and transparent walls, solar irradiation, air infiltration and possible human occupancy. Once the thermal model of an individual room was established, the re-usability and modularity features that distinguish the OOM approach were exploited to create the model of the entire building. Subsequently, the models of heat pump, fan coil and water distribution network were built as well. In the following sections, we detail the model implementation of each of the aforementioned sub-systems, together with the equations and parameters involved.

### 2.1. Rooms and building

Here, the heat transfer mechanisms between a generic room and the surrounding environment were firstly considered. In detail, models to account for the conduction and convection through opaque (i.e., walls, doors, roof and floor) and transparent (i.e., windows) surfaces, the solar irradiance through transparent surfaces and the air ventilation were developed.

The heat flow $\Phi_c$ exchanged by conduction and convection through the building envelope was expressed as [20]:

$$\Phi_c = U \, A \, (T_{int} - T_{ext}), \tag{1}$$

where $T_{int}$ and $T_{ext}$ are respectively the indoor and outdoor temperature of air, $A$ is the heat transfer area, and $U$ is the global heat transfer coefficient. In case of opaque walls, the latter can be computed as [20]:

$$U = \frac{1}{\frac{1}{h_e} + \sum_{n=1}^{N} \frac{s_n}{\lambda_n} + \frac{1}{h_i}}, \tag{2}$$

where $h_i$ and $h_e$ are the indoor and outdoor convection coefficients, respectively, and $s_n$ and $\lambda_n$ the thickness and thermal conductivity of the $n$th layer of the stratigraphy. The thermo-physical properties and geometric characteristics of the walls, floor and doors are reported in Table A.1. Moreover, air convection was considered both indoor ($h_i = 10 \, \frac{W}{m^2 K}$ [21]) and outdoor ($h_e = 40 \, \frac{W}{m^2 K}$, with a conservative hypothesis of near gale wind [22]). In case of windows, the thermal transmittance accounted for both the presence of the glass and the frame surface [23]:

$$U = \frac{A_w (g \, U_g + f \, U_f) + \Psi \, p}{A_w}, \tag{3}$$

where $A_w$ is the total window surface, $g$ and $f = 1 - g$ are the glass and the frame surface portion with respect to the total window surface, $U_g$ and $U_f$ the glass and frame thermal transmittance, respectively. Moreover, $\Psi$ represents the linear thermal transmittance
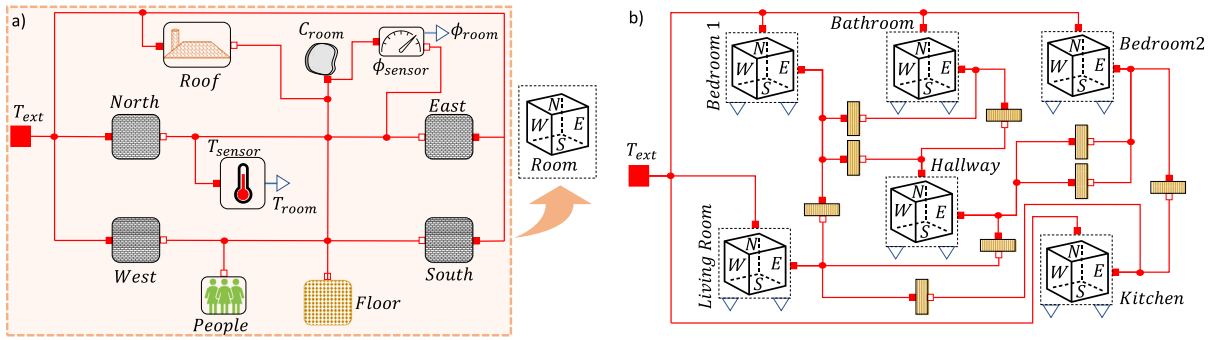
**Fig. 1.** *Modelica* model diagram of (a) a generic room and (b) the considered case study building. The generic room is obtained by connecting the thermal models of four walls (which can include windows and doors), floor, roof and occupants. The model diagram of the building shows all the connection between each room, detailing the presence of indoor walls depicted as brown rectangles. The different components are connected by ports. In detail, the heat ports are represented by the red and white squares, which thus indicate the interface with the potential (here, temperature) and flow (here, heat flow rate) variables, respectively. The outputs (i.e., the temperature of the room $T_{room}$ and the dispersed heat flux $\phi_{room}$) recorded by the temperature and heat flux sensors are represented by the blue and white triangular ports. Note that, various heat sources, such as solar irradiance and air infiltration, are considered and included in the wall model, as discussed in the text. (For interpretation of the references to color in this figure legend, the reader is referred to the web version of this article.)

of the glass edge and $p$ the perimeter of the window. Such specific parameters are reported in Table A.2 for the considered case study.

The incoming radiative (solar) flux $\Phi_r$ exchanged through the glazed surfaces was expressed as [20]

$$\Phi_r = I\, G\, g\, A_w. \tag{4}$$

In Eq. (4), $G$ is the optical G-value of the glass – taken as 0.8 in the considered case study; $I$ is the daily average solar irradiance, whose value is taken from the PVGIS solar radiation database [24,25] depending on the location and period simulated. For the sake of simplicity, no shading factors or corrections due to different solar orientations were considered in the modeled building. Furthermore, the solar heat gain of opaque walls was neglected as a first (conservative) approximation.

Lastly, the heat loss due to ventilation was considered. Assuming, for example, a complete circulation of air every hour for keeping sufficient indoor air quality [26], the minimum air mass flow rate required for the air renewal was computed as $\dot{m}_a = \frac{V}{3600\,\rho}$, where $V$ is the volume of the room and $\rho$ the density of air. The related heat flux $\Phi_v$ due to ventilation was evaluated as [20]

$$\Phi_v = \dot{m}_a\, c_p\, (T_{int} - T_{ext}), \tag{5}$$

being $c_p$ the specific heat capacity of air. Since residential buildings do not typically include mechanical ventilation systems and air change is delegated to manual window openings, here $\Phi_v$ was included in the thermal model of the window.

The *Modelica* model diagram of a generic room implemented in *System Modeler* is reported in Fig. 1(a), where the three different indoor–outdoor heat exchange mechanisms (conduction/convection, ventilation, solar irradiance) are configured in parallel exploiting the electrical analogy. The generic room was defined by four walls (one for each cardinal point), a roof and a floor. Each of these components was equipped with two thermal ports: the red one, connected to the outdoor temperature (i.e., $T_{ext}$); the white one, connected to a heat capacitor element (i.e., $C_{room}$), which accounted for the heat capacity of air in the room. Moreover, the heat capacity of each material in the walls, roof and floor was included in the respective models. The incorporation of a temperature (i.e., $T_{sensor}$) and a heat flux (i.e., $\phi_{sensor}$) sensor allows to keep track of temperature (i.e., $T_{room}$) and dispersed heat flux (i.e., $\phi_{room}$) during the simulated transients. It is worth noting that each wall can be exterior or interior, with or without windows and doors: the implemented model can be readily customized with the actual layout of the considered wall by means of a graphical user interface.

After having modeled the various basic components constituting a generic room, the thermal model of the entire building was properly set up, by taking advantage of the re-usability feature of the object-oriented modeling approach. To this purpose, the layout of the building (namely, the orientation, the geometric characteristics and the number of rooms) should be defined. The layout of the case study under consideration is reported in Fig. A.1 and Table A.3 while the corresponding *System Modeler* model in Fig. 1(b), where the indoor walls (brown rectangles) are connected to the heat capacity of the two adjacent rooms.

### 2.2. Heat pump

The thermal power required by the building was supplied by an air–water heat pump system operating with the R134a refrigerant fluid. First, the required refrigerant mass flow rate was determined. The design ambient temperature was taken as −5 °C, thus the evaporation temperature of the R134a set equal to −10 °C. The water temperature at the condenser outlet (to the fan coil units) was considered equal to 45 °C; therefore, the condensation temperature of the R134a was set to 50 °C. After imposing these design constraints, the cycle was generated using *CoolPack* software. The values of the thermodynamic properties of R134a in the reverse cycle are reported in Table 1.

**Table 1**
Thermodynamic properties of R134a in the reverse cycle of the considered heat pump. $T$, $p$ and $h$ represent the temperature, pressure and enthalpy of the refrigerant fluid.

| STATE | $T$ [°C] | $p$ [bar] | $h$ [$\frac{kJ}{kg}$] |
|---|---|---|---|
| 1 | −10 | 2.007 | 391.32 |
| 2 | 56.2 | 13.176 | 430.32 |
| 3 | 50 | 13.176 | 271.42 |
| 4 | −10 | 2.007 | 271.42 |

The compression stage, during which the refrigerant changes from saturated to super-heated vapor, was represented by the transformation from 1 to 2. Then, the condensation (from 2 to 3), lamination (from 3 to 4) and evaporation (from 4 to 1) processes occur subsequently. The required mass flow rate of refrigerant was computed by a power balance at the condenser:

$$\dot{m}_{r134a} = \frac{\Phi_{tot}}{h_2 - h_3},\tag{6}$$

where $\Phi_{tot}$ is the total thermal load needed by the building in the worst climate condition considered (increased by 20% to be more conservative); whilst, $h_2 - h_3$ is the enthalpy difference in the condenser. The *Modelica* model of heat pump implemented in *System Modeler* receives as input the values of the thermodynamic properties ($p$, $T$, $h$, $s$) of the refrigerant fluid by exploiting the *Coolant Properties* sub-package. Then, the thermal power at the condenser is provided as output of the model, imposing the $\dot{m}_{r134a}$ value.

### 2.3. Fan coil

Air-to-water fan coils were chosen as terminal devices. To reduce the size of the heat exchanger and increase its efficiency, circular fins were applied to the outer surface of the tube containing water [20,27]. A cross-flow configuration between air and water was considered. The procedure outlined in Ref. [20] and based on the $\epsilon - NTU$ method was followed to size the length $L$ of the water tube. Here, the water inlet temperature was fixed to 45 °C and a water–air temperature difference of 10 °C was initially supposed, letting then the system to evolve according to the imposed boundary conditions. The inlet and outlet temperature of air were initially guessed equal to 15 °C and 30 °C, respectively. Then, starting from these temperatures and knowing the maximum thermal power required to heat each room, the water mass flow rate was estimated. Note that, the room requiring the highest thermal power was considered to size the fan coil. For the air mass flow rate, on the other hand, a typical design value (namely, 0.25 kg s$^{-1}$) was selected.

Imposing the diameters of the tube ($d_i$ inner diameter, $d_o$ outer diameter) and the geometric characteristics of the used fins, the hydraulic diameters were calculated at the water and air side, together with the Reynolds ($Re$) number. For the water side $Re >$ 10,000, thus the Dittus–Boelter correlation was resorted to estimate the Nusselt ($Nu$) number:

$$Nu_w = 0.023 \, Re^{0.8} \, Pr^{0.4}.\tag{7}$$

Instead, the correlation proposed by Briggs and Young [28] was considered for the outer air flow on the finned tubes:

$$Nu_a = 0.134 \, Re^{0.681} \, Pr^{\frac{1}{3}} \left(\frac{s - \delta}{b}\right)^{0.2} \left(\frac{s - \delta}{\delta}\right)^{0.113},\tag{8}$$

where $Pr$ is the Prandtl number (calculated considering the properties of the fluid at average temperature, see Table A.4), $s$ the pitch of the fins, $\delta$ and $b$ the thickness and height of the fin, respectively. The convective heat transfer coefficients at the water ($h_w$) and air ($h_a$) side were then computed from $Nu_w$ and $Nu_a$, respectively. The global heat transfer coefficient referred to the water side of fan coil $U_w$ could be eventually calculated as:

$$U_w = \frac{1}{\frac{1}{h_w} + \frac{d_i \ln \frac{d_o}{d_i}}{2\lambda} + \frac{A_i}{A_o h_a \eta}},\tag{9}$$

being $A_i = \pi d_i L$, $A_o = \pi d_o L$, $\lambda$ the thermal conductivity of the tube and $\eta$ the overall fins efficiency. Knowing the heat capacity rate of the two fluids, $\epsilon$, and the flow arrangement, the $NTU$ for both water and air side was finally computed [20]. Hence, the unknown length $L$ of the tube was determined by exploiting the relation $A_i = \frac{NTU_w C_{min}}{U_w}$, being $C_{min}$ the smaller heat capacity rate between the fluids.

The developed *Modelica* model of the fan coil is reported in Fig. 2(a). Such model was implemented in *System Modeler* as a combination of two sub-blocks: *Finned Tube* and *Air Convection*. The *Finned Tube* was designed to account for the heat transfer occurring inside the tube, thus considering the forced convection between water and tube, and the conduction through the tube material. As mentioned, the Dittus–Boelter correlation [20] was implemented to estimate $h_w$ and thus the thermal power transferred between water inside the tube and outer wall. The exchanged thermal power was then communicated, through the white ports showed in Fig. 2(a), to the second component of the model, namely the *Air Convection*. This sub-block accounts for the convection between finned tube and surrounding air, using the Briggs and Young correlation to compute $h_a$. Finally, the thermal connection between the fan coil unit and the room to be heated was established through the red port in Fig. 2(a) (i.e., T), determining the outlet air temperature.
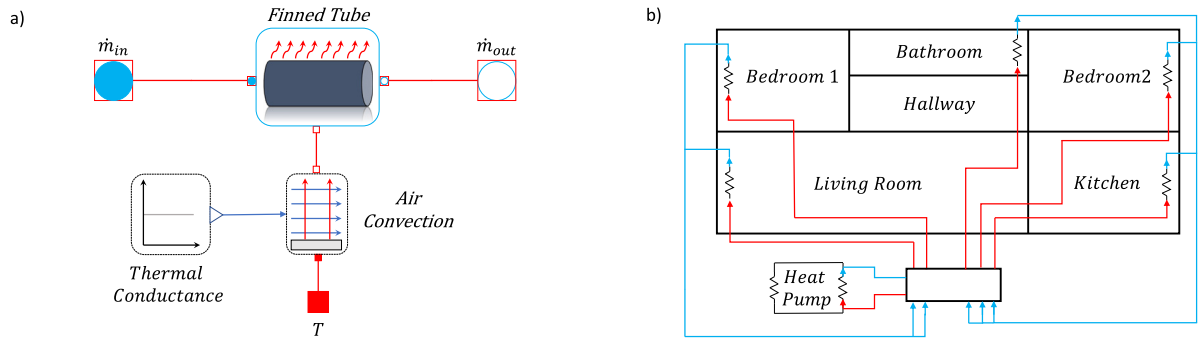
**Fig. 2.** (a) *Modelica* model of the fan coil. The flow ports are represented by the light blue and white circles inscribed in the red boxes (see *Finned Tube* component), which indicate the interface with the potential (here, the pressure and the specific enthalpy) and flow (here, mass and enthalpy flow rate) variables for the fluid flow physics. The *Finned Tube* component shows a heat port (white square), which allows the connection with the *Air Convection* component. (b) Scheme of the water distribution network, consisting of the supply (red lines) and return (blue lines) pipelines. Fan coils and heat exchangers are depicted as thermal resistances. (For interpretation of the references to color in this figure legend, the reader is referred to the web version of this article.)
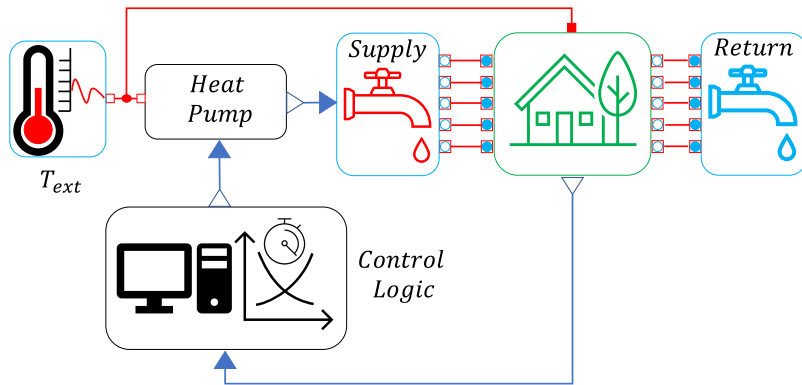


**Fig. 3.** Overall model diagram of the coupling between heating system and building. The *Heat Pump* component is equipped with three ports: the outdoor temperature signal is communicated to the evaporator through the white square port; the heat flux generated in the condenser is forwarded to the distribution network (*Supply* and *Return* components) via the white triangle port; the blue triangle port refers to the control signal from the *Control Logic* component (already available in the *Modelica* library), which allows the heat pump to modulate its operation thus ensuring the desired thermal comfort within the building. (For interpretation of the references to color in this figure legend, the reader is referred to the web version of this article.)

### 2.4. Distribution network

The distribution network of the heat transfer fluid was sized and subsequently modeled in *System Modeler*. As represented in Fig. 2(b), it was composed of two different circuits: the supply (from the condenser of the heat pump to the fan coils) and the return one. First, the layout of these networks was chosen, to estimate the water flow rate and hydraulic head of each pipe. The total water flow rate required was equally partitioned over each branch. However, since different values of thermal power, and therefore water flow rates, were required by each room, balancing valves were included in the network. Both concentrated and distributed losses were considered to choose the water pumping unit. Note that, for more realistic thermal modeling, the effective thermal inertia of each duct, calculated by knowing its geometry and material, was considered. In detail, ducts with outer and inner diameters equal to 20 and 18 mm were taken, respectively.

### 2.5. Overall model

Once all the components of the heating system were modeled and included in the *System Modeler*'s library *College Thermal* [19], the overall model was implemented simply dragging, dropping and connecting these blocks. The model diagram of the entire system is reported in Fig. 3. The obtained system of differential equations was solved with the numerical Runge–Kutta explicit method for all instants of the considered transient: a simulated day required a few minutes of computations by a single AMD Ryzen 5 4600H processor.

The full model represents an efficient tool for simulating and analyzing the heating system and the dynamic thermal response of the building. Each of the blocks in Fig. 3 can be tailored according to the considered case study and their main parameters edited to investigate disparate operating conditions. For instance, the effect of different building geometry, materials of the various
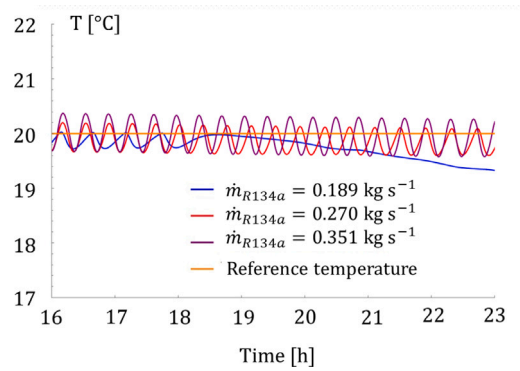
**Fig. 4.** Reference target temperature and actual average indoor air temperature as function of time. Different refrigerant mass flow rates were considered for the heat pump. In detail, the red curve is obtained for $\dot{m}_{R134a} = 0.27$ kg s$^{-1}$, while purple and blue curves with a mass flow rate increased or decreased by 30% from that value, respectively. The reference temperature is represented by the orange line. (For interpretation of the references to color in this figure legend, the reader is referred to the web version of this article.)

components (walls, windows, etc.), system location, thermodynamic cycle of the heat pump, and control strategy on the energy consumption during the heating season could be quickly assessed. As reported in Fig. 3, the outdoor temperature of the selected location was communicated to both models of building and heat pump; then, due to the difference between the target indoor temperature and the ambient one, the *Control Logic* block (i.e., LimPID, which was included in the *Modelica* library) triggers the heating system to operate. The controller was designed to receive the average building temperature signal and, as a set-point, the temperature reference to be ensured within the building, therefore producing a consistent output signal to modulate between a minimum and a maximum value the refrigerant mass flow rate in the heat pump via a PI-type control. In detail, the governing equation of the controller is:

$$u(t) = k \left( e(t) + \frac{1}{T_i} \int_0^t e(\tau) d\tau \right), \tag{10}$$

being $u(t)$ the control signal, $e(t)$ the difference between reference and actual temperature inside the building, and $k$ and $T_i$ the characteristic constants for the proportional and integrative parts.

## 3. Results

The response of the modeled system under different operating conditions was assessed. As a first analysis, the influence of refrigerant mass flow rate was considered to appreciate the importance of a proper heat pump design to guarantee thermal comfort indoor. Then, the dynamic response of the system was tested by varying the main parameters of the PI controller. Finally, the effect of different thermal insulation material or target indoor temperature on the energy consumption of the heating system were checked as well. *Mathematica* was used to analyze and plot results.

### 3.1. Refrigerant mass flow rate effect

The first analysis focused on the effect of the refrigerant mass flow rate (i.e., $\dot{m}_{R134a}$) on the indoor temperature evolution. Without losing generality, the latter was estimated considering a system operating in Milan (Italy) during a realistic heating season. In Fig. 4, the reference target temperature and the actual indoor air temperature evolution are reported as a function of time.

A time window of seven hours was selected to better highlight the different time-fluctuations of temperature, and thus system response, under varying operating conditions. The outdoor temperature (extracted by exploiting *WeatherData* function, which allowed to get real data about the climate condition of Milan) was varied between 5 °C and −3 °C. In Fig. 4, the red curve was obtained for $\dot{m}_{R134a} = 0.27$ kg s$^{-1}$, while purple and blue curves when the flow rate was increased or decreased by 30% from that value, respectively. Results showed that the target air temperature in the building was accurately followed by the heating system for the highest mass flow rate of refrigerant considered (0.351 kg s$^{-1}$, see orange line). Instead, when $\dot{m}_{R134a}$ was decreased, the average indoor temperature started to decay (see orange and blue lines) with time, as the heat pump failed to properly compensate for the heat losses.

### 3.2. PI controller effect

Here, the effect of the PI controller on the transient behavior of the heating system was investigated by varying the gain of the proportional part ($k$) and the integrator time constant ($T_i$) of the controller. In the first scenario, five different values of $k$ were considered (namely, from 0.1 to 1,000), keeping constant $T_i$ (see Fig. 5(a)). The second scenario involved a constant $k$ while $T_i$ varying from 0.01 to 10 s (see Fig. 5(b)).
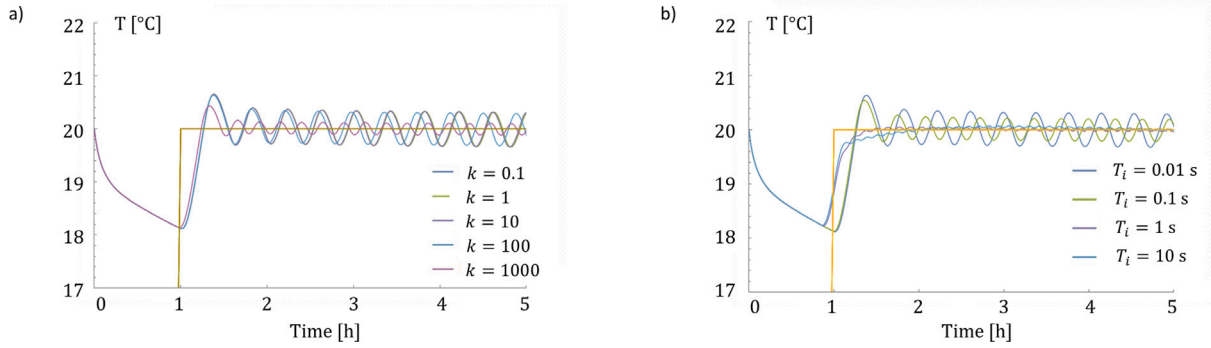
**Fig. 5.** Time-dependent average air temperature in the building as function of (a) the gain $k$ of the proportional part of the PI controller, and (b) the integrator time constant $T_i$ of the PI controller. The reference target temperature is represented by the orange line. (For interpretation of the references to color in this figure legend, the reader is referred to the web version of this article.)
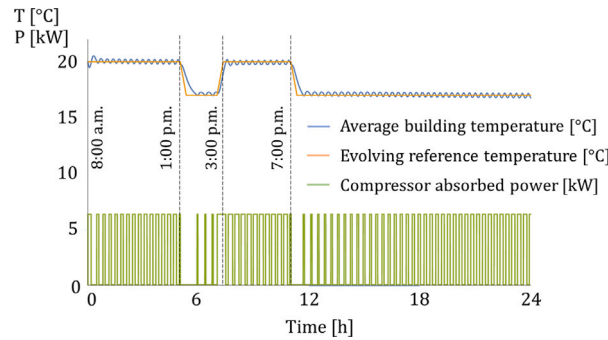


**Fig. 6.** Average air temperature in the building (blue line) and power supplied to the compressor (green line) as function of time, with evolving reference target temperature (orange line). The variation in the reference target temperature reflects the typical daily demand of office workers. (For interpretation of the references to color in this figure legend, the reader is referred to the web version of this article.)

In Fig. 5(a), the temperature transient curves of air in the building resulted to be overlapped with a value of $k$ equal to 0.1, 1 or 10. Whereas, substantial differences were found on the response of the system when $k$ was equal to 100 or 1,000, being higher values of $k$ able to follow the target temperature closely. However, high $k$ values may lead to system instability when quick changes in the outdoor temperature occur. Then, keeping $k$ constant and equal to 500, the second scenario was investigated. Fig. 5(b) highlights how the reference temperature was not properly followed when the time constant was higher than 1 s, while better results were obtained for $T_i$ with values of 0.01 or 0.1 s.

### 3.3. Thermal insulation effect

The energy consumption of the heating system was evaluated by integrating the power absorbed by the compressor over the whole winter season in Milan. Since the energy consumptions of the control and distribution systems are orders of magnitude lower than the compressor one, they are neglected in this case study as a first approximation. In detail, the period from 15 November 2020 to 15 February 2021 was considered. The outdoor temperatures related to this range were obtained by the *WeatherData* function of *Mathematica*, which provides the recorded climatic data for the considered location in the specified period. The resulting energy consumption accounted for 34,850 MJ.

Then, a scenario involving an additional thermal envelope applied on the external surface of the building was considered as well, to quantify the possible energy savings from more thermally insulating walls. In detail, a layer of rock wool was chosen for the additional insulating layer ($\lambda = 0.037$ $\frac{W}{mK}$, $s = 0.05$ m). As a result, the thermal transmittance of the wall was reduced by 60%, namely from 1.155 to 0.451 [$\frac{W}{m^2K}$]. This led to significant energy savings, requiring about 45% less energy (namely, 19,247 MJ) over the entire winter season with respect to the reference case study.

### 3.4. Indoor timer effect

A timer may be exploited to vary the indoor reference temperature as needed during the day, thus reducing the energy consumption of the heating system. Here, the following daily demand was considered as a case study: a higher reference temperature equal to 20 °C from 8:00 a.m. to 1:00 p.m., and from 3:00 p.m. to 7:00 p.m.; whereas, a lower reference temperature (here, 17 °C

**Table A.1**

Density, thermal conductivity, thickness and specific heat capacity of the modeled case study of the wall, floor and door.

| Layer | $\rho$ [$\frac{kg}{m^3}$] | $\lambda$ [$\frac{W}{mK}$] | $s$ [m] | $c$ [$\frac{J}{kgK}$] |
|---|---|---|---|---|
| External wall insulation | 90 | 0.037 | 0.02 | 1030 |
| Inner wall material | 1681 | 0.6 | 0.05 | 840 |
| Internal wall insulation | 410 | 0.086 | 0.01 | 1000 |
| Floor material | 1680 | 0.07 | 0.05 | 840 |
| Door material | 500 | 0.13 | 0.06 | 1600 |

was set without losing generality) from 1:00 p.m. to 3:00 p.m. and after 7:00 p.m. The reference temperature transient, together with the simulation results, are reported in Fig. 6. The power absorbed by the compressor is represented by the green line, whilst the blue and the orange lines refer to the average air temperature in the building and the reference target temperature, respectively. Results in Fig. 6 showed that the modeled heating system could quickly adapt to the variation in the reference target temperature (see, e.g., after 1:00 p.m.) by tuning the refrigerant mass flow rate and thus power absorbed by the heat pump compressor.

## 4. Conclusions

The acausal equation-based and object-oriented modeling approach allows a broader understanding and reliable prediction of the behavior of multi-physical engineering systems with varying degrees of complexity. Here, the new object-oriented model library *College Thermal* purpose-built for thermodynamic systems was proposed to study an heating system. Such library makes use of *Modelica* language, and it is deployed in the *Wolfram System Modeler* environment [19]. The case study simulation required defining the characteristics of (a) building (such as the number and size of rooms, the features of transparent and opaque walls, etc.), (b) heat pump, (c) fan coil units, and (d) water distribution network. To this purpose, tailored dynamic models with lumped parameters were created, to represent the heat and mass transfer phenomena involved in the aforementioned components. As a result, a fully integrated environment for analyzing the system energy performance was assembled. In detail, transient simulations of a heating system were performed to test its energy performance and transient response under different operating conditions, PI control strategies, building characteristics and user needs.

In perspective, tuning the thermodynamic cycle of heat pump to summer conditions would allow the reuse of the same lumped-element model in cooling systems as well. In such summer conditions, the lumped-element models of the distribution system, fan coil and building would still work too. Instead, new lumped-element models considering humid air properties and transformations (e.g., humidifiers, dehumidifiers, fans) should be developed to control the air humidity too. Thanks to a simple integration with the *Modelica* libraries readily available in the *Wolfram System Modeler* software, the modeling approach and the library presented in this work may allow to expeditiously study various heating and cooling system designs, providing a valuable tool for quick component selection in complex thermal systems, eventually including thermal energy storage [29] and solar thermal energy supply [30,31].

**CRediT authorship contribution statement**

**Luigi Augello:** Methodology, Software, Formal analysis, Investigation, Data curation, Writing – original draft, Visualization. **Ankit Naik:** Methodology, Software, Formal analysis, Writing – Original Draft, Visualization. **Matteo Morciano:** Validation, Formal analysis, Writing – review & editing, Visualization. **Jan Brugård:** Resources, Formal analysis, Writing – review & editing, Supervision, Project administration. **Matteo Fasano:** Conceptualization, Formal analysis, Writing – review & editing, Supervision, Project administration.

**Declaration of competing interest**

The authors declare that they have no known competing financial interests or personal relationships that could have appeared to influence the work reported in this paper.

**Data availability**

Data will be made available on request.

**Appendix**

See Tables A.1–A.4 and Fig. A.1.

**Table A.2**
Parameters for evaluating the thermal and optical performance of the windows in the considered case study.

| $A_w[\text{m}^2]$ | $g[-]$ | $f[-]$ | $\Psi[\frac{\text{W}}{\text{mK}}]$ | $U_g[\frac{\text{W}}{\text{m}^2\text{K}}]$ | $U_f[\frac{\text{W}}{\text{m}^2\text{K}}]$ | $p[\text{m}]$ |
|---|---|---|---|---|---|---|
| 3.2 | 0.8 | 0.2 | 0.06 | 1.6 | 1.8 | 7.2 |

**Table A.3**
Geometric characteristics of each room in the proposed building for the case study.

| Room | Length [m] | Width [m] | Height [m] |
|---|---|---|---|
| Living room | 8 | 5 | 3 |
| Kitchen | 4 | 5 | 3 |
| Bed room 1 | 4 | 5 | 3 |
| Bed room 2 | 4 | 5 | 3 |
| Bath room | 4 | 3 | 3 |
| Hallway | 4 | 2 | 3 |

**Table A.4**
Properties of the fluids in the heating system case study.

| Parameter | Water | Air |
|---|---|---|
| $\mu$ [Pa s] | $6.53 \cdot 10^{-4}$ | $1.81 \cdot 10^{-5}$ |
| $\lambda$ [$\frac{\text{W}}{\text{mK}}$] | 0.6 | 0.026 |
| $c_p$ [$\frac{\text{J}}{\text{kgK}}$] | 4186 | 1005.5 |
| $\rho$ [$\frac{\text{kg}}{\text{m}^3}$] | 992.2 | 1.205 |
| $\Delta p$ [kPa] | 5 | 8.79 |
| $Pr$ [$-$] | 4.56 | 0.70 |



**Fig. A.1.** Layout of the proposed building for the case study.

## References

[1] K. Voss, E. Musall, M. Lichtmeß, From low-energy to net zero-energy buildings: Status and perspectives, J. Green Build. 6 (1) (2011) 46–57.
[2] M. Irfan, N. Abas, M.S. Saleem, Thermal performance analysis of net zero energy home for sub zero temperature areas, Case Stud. Therm. Eng. 12 (2018) 789–796.
[3] K. Sudhakar, M. Winderl, S.S. Priya, Net-zero building designs in hot and humid climates: A state-of-art, Case Stud. Therm. Eng. 13 (2019) 100400.
[4] Z. Afroz, G. Shafiullah, T. Urmee, G. Higgins, Modeling techniques used in building HVAC control systems: A review, Renew. Sustain. Energy Rev. 83 (2018) 64–84.
[5] S. Attia, E. Gratia, A. De Herde, J.L. Hensen, Simulation-based decision support tool for early stages of zero-energy building design, Energy Build. 49 (2012) 2–15.
[6] M. Wetter, Modelica-based modelling and simulation to support research and development in building energy and control systems, J. Build. Perform. Simul. 2 (2) (2009) 143–161.
[7] M. Trčka, J.L. Hensen, Overview of HVAC system simulation, Autom. Constr. 19 (2) (2010) 93–99.
[8] P. Li, Y. Li, J.E. Seem, H. Qiao, X. Li, J. Winkler, Recent advances in dynamic modeling of HVAC equipment. Part 2: Modelica-based modeling, HVAC R Res. 20 (1) (2014) 150–161.

[9] V.B. Kopei, R. Onysko, V.G. Panchuk, Component-oriented acausal modeling of the dynamical systems in Python language on the example of the model of the sucker rod string, PeerJ Comput. Sci. 5 (2019) e227.

[10] P. Fritzson, V. Engelson, Modelica—A unified object-oriented language for system modeling and simulation, in: European Conference on Object-Oriented Programming, Springer, 1998, pp. 67–90.

[11] A.A.W. Hawila, A. Merabtine, N. Troussier, S. Mokraoui, A. Kheiri, A. Laaouatni, Dynamic model validation of the radiant floor heating system based on the object oriented approach, in: 2016 International Renewable and Sustainable Energy Conference, IRSEC, IEEE, 2016, pp. 275–280.

[12] H. Elmqvist, A Structured Model Language for Large Continuous Systems (Ph.D. thesis), Universiteit i Lund, 1978.

[13] S. Heinke, C. Pereira, S. Leonhardt, M. Walter, Modeling a healthy and a person with heart failure conditions using the object-oriented modeling environment dymola, Med. Biol. Eng. Comput. 53 (10) (2015) 1049–1068.

[14] D. Brück, H. Elmqvist, S.E. Mattsson, H. Olsson, Dymola for multi-engineering modeling and simulation, in: Proceedings of Modelica, Vol. 2002, Citeseer, 2002.

[15] R. Franke, Object-oriented modeling of solar heating systems, Sol. Energy 60 (3–4) (1997) 171–180.

[16] J. Bansiya, C.G. Davis, A hierarchical model for object-oriented design quality assessment, IEEE Trans. Softw. Eng. 28 (1) (2002) 4–17.

[17] J. Rosenow, D. Gibb, T. Nowak, R. Lowes, Heating up the global heat pump market, Nat. Energy 7 (10) (2022) 901–904.

[18] O. Montero, P. Brischoux, S. Callegari, C. Fraga, M. Ruetschi, E. Vionnet, N. Calame, F. Rognon, M. Patel, P. Hollmuller, Large air-to-water heat pumps for fuel-boiler substitution in non-retrofitted multi-family buildings—energy performance, $CO_2$ savings, and lessons learned in actual conditions of use, Energies 15 (14) (2022) 5033.

[19] System modeler modelica library store: College thermal, 2022, https://www.wolfram.com/system-modeler/libraries/college-thermal/. (Accessed 03 August 2022).

[20] R.K. Shah, D.P. Sekulic, Fundamentals of Heat Exchanger Design, John Wiley & Sons, 2003.

[21] E.F. Daniel, O.P. Curtis, Convective energy and heat transfer thermal load in building calculations, ASHRAE Trans. 103 (2) (1997).

[22] M.G. Emmel, M.O. Abadie, N. Mendes, New external convective heat transfer coefficient correlations for isolated low-rise buildings, Energy Build. 39 (3) (2007) 335–342.

[23] P. Blanusa, W.P. Goss, H. Roth, P. Weitzmannn, C.F. Jensen, S. Svendsen, H. Elmahdy, Comparison between ashrae and iso thermal transmittance calculation methods, Energy Build. 39 (3) (2007) 374–384.

[24] E. PVGIS, Photovoltaic geographical information system, línea, 2018, Available: https://rejrc.ec.europa.eu/pvg_tools/es/#PVP.

[25] A. Bocca, L. Bottaccioli, E. Chiavazzo, M. Fasano, A. Macii, P. Asinari, Estimating photovoltaic energy potential from a minimal set of randomly sampled data, Renew. Energy 97 (2016) 457–467.

[26] R. American Society of Heating, A.-C. E. (ASHRAE), Ventilation and acceptable indoor air quality in residential buildings, 2016.

[27] A. Ciuffini, A. Scattina, F. Carena, M. Roberti, G. Toscano Rivalta, E. Chiavazzo, M. Fasano, P. Asinari, Multiscale computational fluid dynamics methodology for predicting thermal performance of compact heat exchangers, J. Heat Transfer 138 (7) (2016).

[28] A. Bejan, A.D. Kraus, Heat Transfer Handbook, Vol. 1, John Wiley & Sons, 2003.

[29] A. Ribezzo, G. Falciani, L. Bergamasco, M. Fasano, E. Chiavazzo, An overview on the use of additives and preparation procedure in phase change materials for thermal energy storage with a focus on long term applications, J. Energy Storage 53 (2022) 105140.

[30] M. Morciano, M. Fasano, M. Secreto, U. Jamolov, E. Chiavazzo, P. Asinari, Installation of a concentrated solar power system for the thermal needs of buildings or industrial processes, Energy Procedia 101 (2016) 956–963.

[31] A. Bologna, M. Fasano, L. Bergamasco, M. Morciano, F. Bersani, P. Asinari, L. Meucci, E. Chiavazzo, Techno-economic analysis of a solar thermal plant for large-scale water pasteurization, Appl. Sci. 10 (14) (2020) 4771.